Selective Inhibition of Angiogenesis in Small Blood Vessels and Decrease in Vessel Diameter throughout the Vascular Tree by Triamcinolone Acetonide

Terri L. McKay,[1] *Dan J. Gedeon,*[1] *Mary B. Vickerman,*[1] *Alan G. Hylton,*[1] *Daniela Ribita,*[1] *Harry H. Olar,*[1] *Peter K. Kaiser,*[2] *and Patricia Parsons-Wingerter*[1]

Purpose. To quantify the effects of the steroid triamcinolone acetonide (TA) on branching morphology within the angiogenic microvascular tree of the chorioallantoic membrane (CAM) of quail embryos.

Methods. Increasing concentrations of TA (0–16 ng/mL) were applied topically on embryonic day (E) 7 to the chorioallantoic membrane (CAM) of quail embryos cultured in petri dishes and incubated for an additional 24 or 48 hours until fixation. Binary (black/white) microscopic images of arterial end points were quantified by generational analysis of vessel branching (VESGEN) software to obtain major vascular parameters that include vessel diameter (D_v), fractal dimension (D_f), tortuosity (T_v), and densities of vessel area, length, number, and branch point (A_v, L_v, N_v, and Br_v). For assessment of specific changes in vascular morphology induced by TA, the VESGEN software automatically segmented the vascular tree into branching generations ($G_1 \ldots G_{10}$) according to changes in vessel diameter and branching.

Results. Vessel density decreased significantly up to 34% as the function of increasing concentration of TA according to A_v, L_v, Br_v, N_v, and D_f. TA selectively inhibited the growth of new, small vessels because L_v decreased from 13.14 ± 0.61 cm/cm^2 for controls to 8.012 ± 0.82 cm/cm^2 at 16 ng TA/mL in smaller branching generations (G_7–G_{10}) and for N_v from 473.83 ± 29.85 cm^{-2} to 302.32 ± 33.09 cm^{-2}. In contrast, vessel diameter (D_v) decreased throughout the vascular tree (G_1–G_{10}).

Conclusions. By VESGEN analysis, TA selectively inhibited the angiogenesis of smaller blood vessels, but decreased the vessel diameter of all vessels within the vascular tree. (*Invest Ophthalmol Vis Sci.* 2008;49:1184–1190) DOI:10.1167/iovs.07-1329

The steroid triamcinolone acetonide (TA) is a potent anti-inflammatory and antiangiogenic drug used for the treatment of macular edema secondary to retinal vascular diseases, including diabetic retinopathy and retinal vascular occlusions, and of neovascularization, including choroidal neovascularization (CNV) and retinal neovascularization in inflammatory diseases. It is believed that corticosteroids decrease levels of retinal thickening and improve macular edema by several mechanisms. TA decreases inflammatory mediators that include tumor necrosis factor, interleukin 5, interleukin 6, interleukin 8, prostaglandins, and interferon-gamma.[1–3] TA modulates cellular calcium levels by interacting with voltage-dependent calcium channels and calmodulin.[4,5] These activities may promote more effective fluid resorption, resulting in decreased macular edema. Corticosteroids also decrease levels of the potent permeability factor, vascular endothelial growth factor (VEGF).[6,7] Finally, TA improves the integrity of the blood-retinal barrier.[8] Regardless of the mechanisms of activity, TA has been documented to significantly improve vision and decrease retinal edema.[9–12]

Although the clinical effect of TA in these diseases is established, the effect of TA on vascular morphology is not well understood. Improved understanding of how TA affects angiogenesis and vascular morphology would be helpful for therapeutic optimization. For this study, site-specific changes within the vascular tree induced by TA were quantified using an in vivo model of angiogenesis.

For evaluation of the effects of TA on the angiogenic vascular tree, the quail chorioallantoic membrane (CAM) is a highly useful model during mid-development, when the rate of CAM angiogenesis is at a maximum.[13–17] As described previously, the complex spatial patterns of the branching vascular tree and the associated capillary network can be easily visualized by light and fluorescence/confocal microscopy.[13–17] Using fractal analysis, this vascular pattern can be precisely analyzed. Fractal analysis is a recent non-Euclidean mathematical innovation[18] that quantifies the space-filling patterns of complex objects. Fractal geometry is common in nature and includes botanical and vascular trees, snowflakes, coastline topography, and even the spatiotemporal scaling of vascular-based physiological metabolism.[19,20] As a fractional, nonintegral number that increases according to the increasing density of a space-filling pattern, the fractal dimension (D_f) is statistically sensitive to small, early-stage changes in the vascular tree.[13–15,17,21] A fractal object typically reaches its greatest space-filling capacity using self-similarity, the geometric property by which a pattern such as vascular bifurcational branching is repeated iteratively at continuously decreasing length scales.

The computer program VESGEN (abbreviated from generational analysis of vessel branching) was developed by the National Aeronautics and Space Administration (NASA) as a fully automated, user-interactive program that quantifies major vascular branching parameters using a single, user-provided image of two-dimensional (2D) vascular pattern. The fractal-based VESGEN analysis segments vessels within vascular trees into branching generations (G_1, G_2, $\ldots$ G_x) according to changes in vessel diameter and branching. Site-specific changes within the vascular tree induced by angiogenic cyto-

From the [1]Research & Technology Directorate and National Center for Space Exploration Research, NASA Glenn Research Center, Cleveland, Ohio; and the [2]Cole Eye Institute, Cleveland Clinic Foundation, Cleveland, Ohio.

Supported by National Eye Institute Grants R01EY17529 (PP-W) and R01EY17528 (PKK) and by NASA Glenn Internal Research and Development Award IRD04–54 (PP-W).

Submitted for publication October 16, 2007; accepted January 21, 2008.

Disclosure: **T.L. McKay**, None; **D.J. Gedeon**, None; **M.B. Vickerman**, P; **A.G. Hylton**, None; **D. Ribita**, None; **H.H. Olar**, None; **P.K. Kaiser**, P; **P. Parsons-Wingerter**, P

The publication costs of this article were defrayed in part by page charge payment. This article must therefore be marked "*advertisement*" in accordance with 18 U.S.C. §1734 solely to indicate this fact.

Corresponding author: Patricia Parsons-Wingerter, Research & Technology Directorate and National Center for Space Exploration Research, NASA Glenn Research Center, MS 110-3, Cleveland, OH 44135; patricia.parsons@grc.nasa.gov.

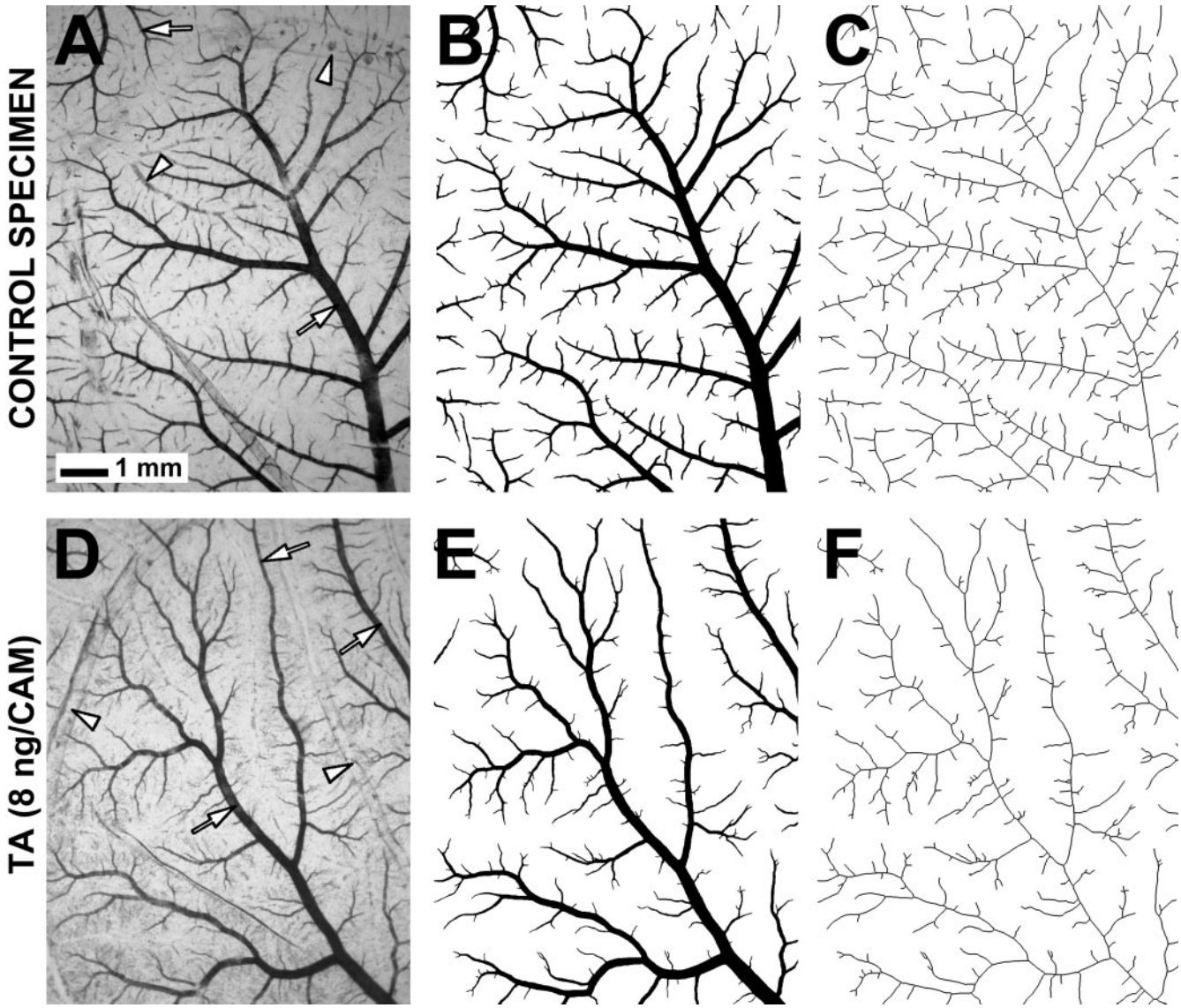

FIGURE 1. Image analysis. Representative images of arterial end point regions of CAM specimens treated with PBS control vehicle (**A**) or with corticosteroid TA (**D**) were acquired by brightfield microscopy. Aldehyde fixation of the CAM results in retention of RBCs within arterial vessels (*arrows*) and extraction of large amounts of blood from venous vessels (*arrowheads*). Arterial trees are thereby conveniently separated from overlapping venous trees to support the semiautomatic processing of grayscale images into (**B**, **E**) binary (black/white) vascular patterns. Binary images and (**C**, **F**) corresponding skeletonized images clearly reveal strong inhibition of vessel density by TA. Measurements of decreased vessel density at 8 ng TA/CAM (**E**, **F**) relative to control (**B**, **C**) include (**E**) vessel area density (A_v) = 0.122 (cm^2/cm^2) and fractal dimension (D_f) = 1.656 compared with (**B**) A_v = 0.152 (cm^2/cm^2) and D_f = 1.683; (**F**) vessel length density (L_v) = 20 (cm/cm^2), vessel branch-point density (Br_v) = 325 (cm^{-2}), and D_f = 1.360 compared with (**C**) L_v = 26 (cm/cm^2), Br_v = 443 (cm^{-2}), and D_f = 1.410.

kines or other molecular regulators, such as TA, can then quantified.[14–16] Thus, the purpose of this study was to evaluate the effects of the TA on branching morphology within the microvascular tree of the quail CAM model using fractal-based VESGEN analysis.

MATERIALS AND METHODS

Embryonic culture, assay, mounting, imaging, and fractal/VESGEN branching analysis used in this study have been described previously[14–17] and are summarized here.

Culture, Assay, and Mounting

Fertilized eggs of Japanese quail (*Coturnix coturnix japonica*, Boyd's Bird Co., Pullman, WA) were incubated at 37.6° ± 0.2°C under ambient atmosphere, cracked at embryonic day 3 (E3; after incubation of eggs for 56 hours), and cultured further in six-well petri dishes (cross-sectional area, 10 cm^2). Quail egg culture and experimental protocols were in accordance with National Institutes of Health guidelines and approved by the Chief Veterinarian Officer of NASA (Ames Research Center). At E7 (after incubation for an additional 96 hours), prewarmed PBS solution containing TA (0.5 mL at 0–16 ng/mL) was applied dropwise to the surface of each CAM. Sterile-filtered stock solutions of TA (T-6501; Sigma, St. Louis, MO) were prepared at 10 mg/mL in 100% ethanol. Additional concentrations of TA were tested to determine the range of dose effectiveness. The total amount of the molecular regulator, rather than its concentration, is the governing parameter because solutions are quickly absorbed into CAM tissue. Quantities of TA are therefore reported as 0 to 8 ng/CAM. After treatment with TA and further incubation for 24 or 48 hours, the embryos (with CAMs) were

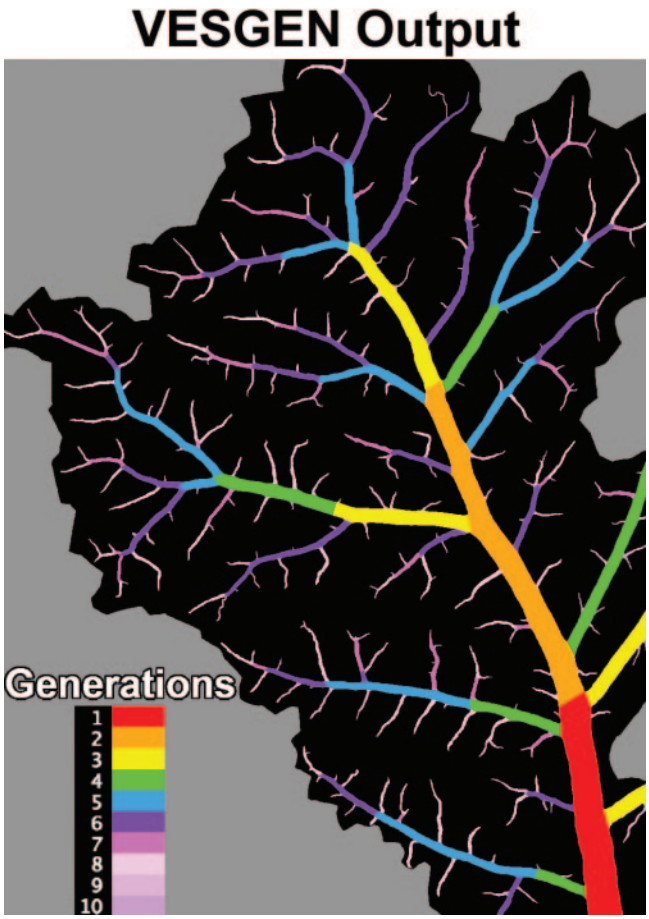

FIGURE 2. Assignment of vessels to branching generations G_1–G_{10} by VESGEN. The VESGEN output image of a CAM control specimen illustrates the classification of vessels into ten successively smaller branching generations (G_1–G_{10}) for the arterial end point region. Vessel branching generations are determined by (1) decrease in vessel diameter and (2) vessel bifurcations that are approximately symmetric (i.e., when diameters of offspring vessels branching from a parent vessel are approximately equal). The major arterial tree and its corresponding ROI (*black*) are also identified by VESGEN. The edge of the ROI lies midway between the end points of the major arterial tree and neighboring arteries. Where vessels of the arterial tree extend beyond the edge of the image, the ROI is defined simply by the edge of the image. The most frequent branching event within the vascular tree is asymmetric branching or branching of a small offshoot vessel from a much larger vessel. In this ROI, 35 symmetric branch points and 209 asymmetric branch points were measured by VESGEN.

fixed in 4% paraformaldehyde/2% glutaraldehyde/PBS for several days before dissection and mounting for microscopic analysis.[13]

Imaging

Aldehyde fixation of the CAM results in high contrast of the arterial tree because of retention of erythrocytes (red blood cells [RBCs]) within arteries but low contrast of the venous tree resulting from evacuation of RBC from veins during dissection (Fig. 1).[13] Digital images (1392 × 1040 pixels) of (terminal) arterial end point vessels from the middle region of the CAM were acquired in grayscale (0–255 intensity) at total 12.5× magnification and resolution of 7.32 μm/pixel (DM4000B microscope [Leica, Wetzlar, Germany] attached to a Retiga EXi CCD camera [Qimaging; Image Pro Plus software]). Previous studies showed that the CAM arterial end point regions analyzed by us are representative of changes induced by topical application of angiogenesis regulators throughout the CAM arterial trees,[13] and that there is no significant increase in vascular density at a total magnification of 20× in comparison with 12.5×. Grayscale images were converted to binary (black/white) images of vascular morphology (Fig. 1) by semiautomatic computer processing using Adobe Photoshop 7.0 and NIH ImageJ software (http://rsb.info.nih.gov/ij/). The accuracy of vascular image binarization was confirmed by a second independent, experienced operator.

Vascular Quantification

Statistical Sampling. Thirty-nine representative CAM specimens were quantified from three independent experiments, including at least three controls from each experiment (a total of 11 controls) and seven specimens for each of the four concentrations of TA. Additional specimens and experiments served as qualitative confirmation of the quantified results. Variation was assessed by calculating the SE. *P* values were obtained for the four treatment groups (1–8 ng TA/CAM) compared to control (0 ng TA/CAM) by two-tailed, heteroscedastic Student's *t*-test.

Analysis by VESGEN. The NASA Glenn computer code VESGEN (Fig. 2) was used to measure parameters of vascular morphology that included vessel length density (L_v), vessel area density (A_v), vessel branch point density (Br_v), vessel number density (N_v), vessel tortuosity (T_v) and vessel diameter (D_v) for each branching generation G_1 through G_{10}. For example, D_{v1-2} denotes D_v with respect to branching generations G_1–G_2. By VESGEN analysis, only one image was found to contain 11 branching generations (i.e., a few vessels of G_{11}), which were therefore merged into image results for G_{7-10} ($G_{\geq 7}$). L_v, A_v, N_v, and Br_v were expressed as density functions by normalization to the area of the image containing the major arterial tree extracted as region of interest (ROI) or the entire image (Fig. 2). Vessel diameter was calculated as $D_v = A_v/L_v$. A trimmed skeleton was used to obtain accurate measurements for L_v in specific branching generations such as L_{v1}.[16] Tortuosity (T_v) was estimated by the ratio of the length of a trimmed vessel (L_v) determined by VESGEN to the shortest distance between the vessel end points.

Vessel branching generations (G_1–G_X) are determined by VESGEN according to relative decreases in vessel diameter, as first established for branching vascular trees in the dog and pig heart and lung.[22–24] Blood flow is conserved at a symmetric vessel bifurcation when the diameter of a symmetric offspring vessel decreases to 71% ($1/\sqrt{2}$) of the parent vessel diameter; therefore, the decrease of vessel diameter to 71% was used as the primary determinant of a new branching generation. As can be seen in biological branching trees (Fig. 2), however, the branching of relatively symmetric offspring vessels is not perfectly symmetric, and the diameters of few offspring vessels are of the ideal 71% value. In addition, vessels tend to taper. To accommodate a range of vessel diameters within a branching generation, VESGEN contains a 15% default tolerance factor that is user adjustable. For the TA study, the tolerance factor was left at ±15%. For a small number of vessel segments (only five vessel segments within 39 total images), the automatic segmentation by VESGEN was incorrect according to the established criteria of generational classification based on vessel diameter and branching. The user-interactive features of VESGEN were therefore used to override and correct these few inaccuracies. A further consideration is that the most frequent branching event in a vascular tree is the asymmetric offshoot branching of a much smaller vessel from a larger vessel, presumably because of space-filling requirements of vascular branching (Fig. 2). It is important to note that although the branching pattern of each vascular tree in a CAM or a human retina is unique, the space-filling properties of the vascular trees are remarkably uniform.[13,21]

VESGEN now functions as a fully automated Java-based software operating as a plug-in to NIH ImageJ. A binary vascular image is the single input required by VESGEN to quantify vascular trees, networks, or tree-network composites of highly 2D tissues such as the avian CAM, human retina, and rodent retina. VESGEN will be publicly available in the near future, and its full capabilities are being described elsewhere.

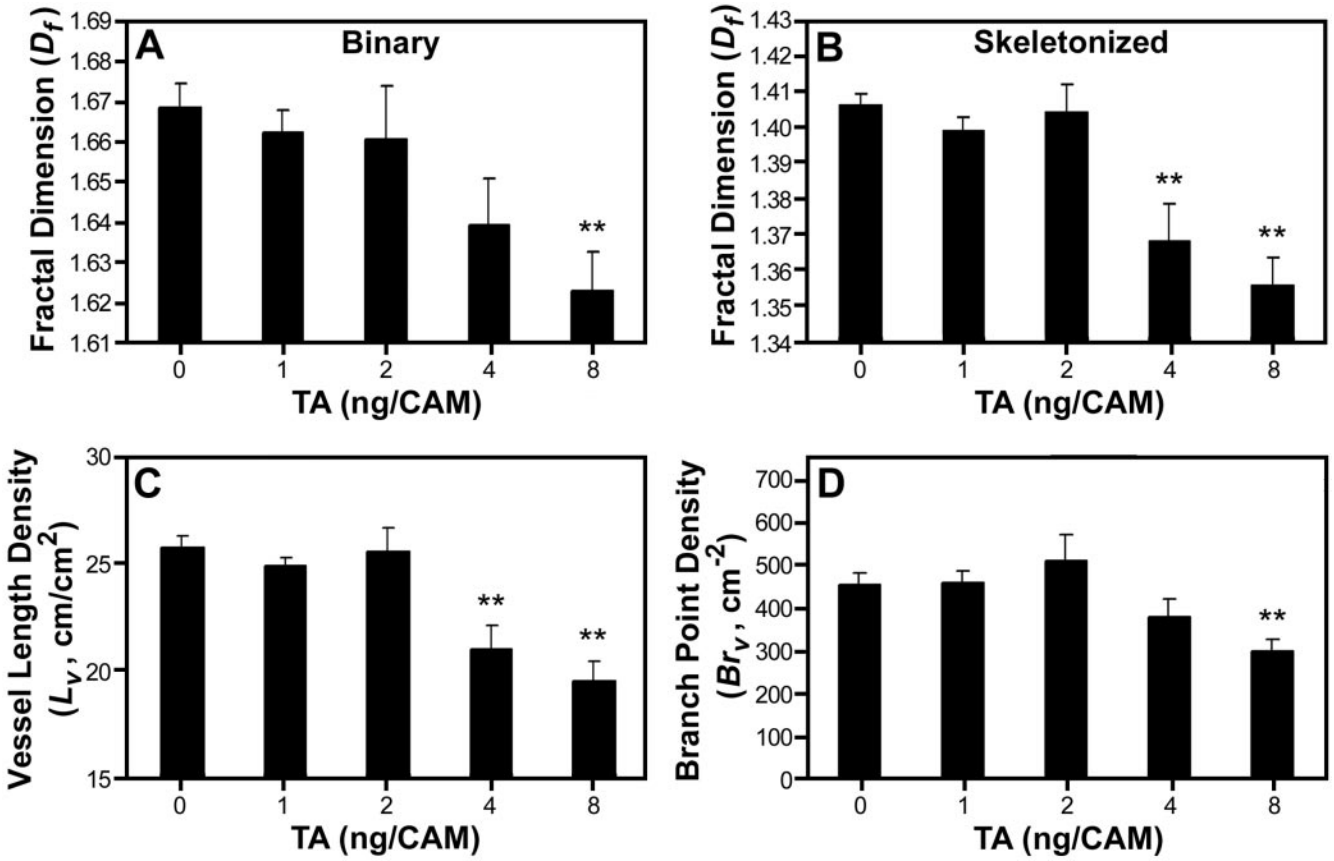

FIGURE 3. Vessel density decreases as the function of increasing concentration of TA. As a measure of the space-filling capacity of a vascular pattern, the fractal dimension (D_f) decreased significantly with increasing TA concentration in (**A**) binary and (**B**) skeletonized images throughout the entire vascular field, as illustrated in Figure 1. Vessel density also decreased according to other measures of vessel density that include (**C**) vessel length density (L_v) and (**D**) vessel branch point density (Br_v). Data are plotted as mean ± SE. $^*P \leq 0.05$. $^{**}P \leq 0.01$.

Fractal Analysis. To support fractal analysis by the box-counting algorithm,[13] each binary image was rescaled slightly to 1370 × 1024. A left- and right-most square image of 1024 × 1024 was extracted from each binary image and skeletonized (i.e., linearized; Fig. 1) using the NIH ImageJ skeletonizing algorithm. The fractal dimension (D_f) was calculated for binary and skeletonized images by implementation of box-counting at a power of 2 using ImageJ.[13] Values of D_f for the left and right 1024 × 1024 images were averaged to obtain an overall D_f for each original image. The fractal box-counting algorithm has since been incorporated into VESGEN to confirm the TA fractal results and for use in future studies. We consider VESGEN to be a fractal-based analysis of vascular trees because of the complex, non-Euclidean space-filling geometry of the vascular branching structures and VESGEN assignment of vascular parameters to specific, self-similar generations of vascular branching.

RESULTS

Topical application of TA significantly inhibited ongoing angiogenesis in the quail CAM after 24 hours by two major morphologic mechanisms: vascular density was inhibited by a targeted decrease in the number of small blood vessels, and vessel diameter was decreased throughout the vascular tree. Vascular density decreased as a function of increasing concentration of TA (Fig. 3) by several confirming measures of the entire vascular field in binary and skeletonized images that include D_f, L_v, and Br_v. Skeletonized images are direct representations of vessel density that illustrate the extensive space-filling properties and overall vessel connectivity of a branching vascular tree. Visual inspection of vascular pattern further confirms these results (Figs. 1, 4). By microscopic observation, decreased vascular density and alterations in vessel diameter induced by TA at 4 to 8 ng/CAM persisted after 48 hours (results not shown).

Within skeletonized images, L_v and Br_v decreased up to 23% and 34%, respectively (Fig. 3). D_f, L_v, and Br_v decreased from 1.406 ± 0.004, 25.7 ± 0.6 (cm/cm^2), and 454 ± 28 (cm^{-2}) in controls to 1.355 ± 0.008, 19.5 ± 0.9 (cm/cm^2), and 301 ± 27 (cm^{-2}) in specimens treated at the maximum concentration of 8 ng TA/CAM (P = 3xE-4, 1xE-4, and 0.001, respectively). In binary images, D_f and A_v decreased from 1.669 ± 0.006 and 0.14 ± 0.00 (cm^2/cm^2) in controls to 1.623 ± 0.009 and 0.11 ± 0.005 (cm^2/cm^2) at 8 ng TA/CAM (P = 0.0015 and 6xE-4). Absolute differences of D_f in binary and skeletonized images may appear small. However, as a non-Euclidean, "fractional" measure of space-filling patterns, D_f is restricted in 2D, black/white images to fractional values between 1 and 2. D_f is a sensitive, statistically significant, reproducible measure of space-filling vascular density that ranges from approximately 1.34 to 1.55 in skeletonized images and 1.61 to 1.75 in binary images.[13–15,17,21]

Decreases in vascular density as measured by D_f and A_v in binary images can result from several morphologic changes that include decreased vessel length and number of vessels and/or decreased vessel diameter (Figs. 1B, 1E). Quantitative analysis by VESGEN confirmed visual observations that the morphologic mechanisms of decreased vascular density induced by TA included the decreased number densities re-

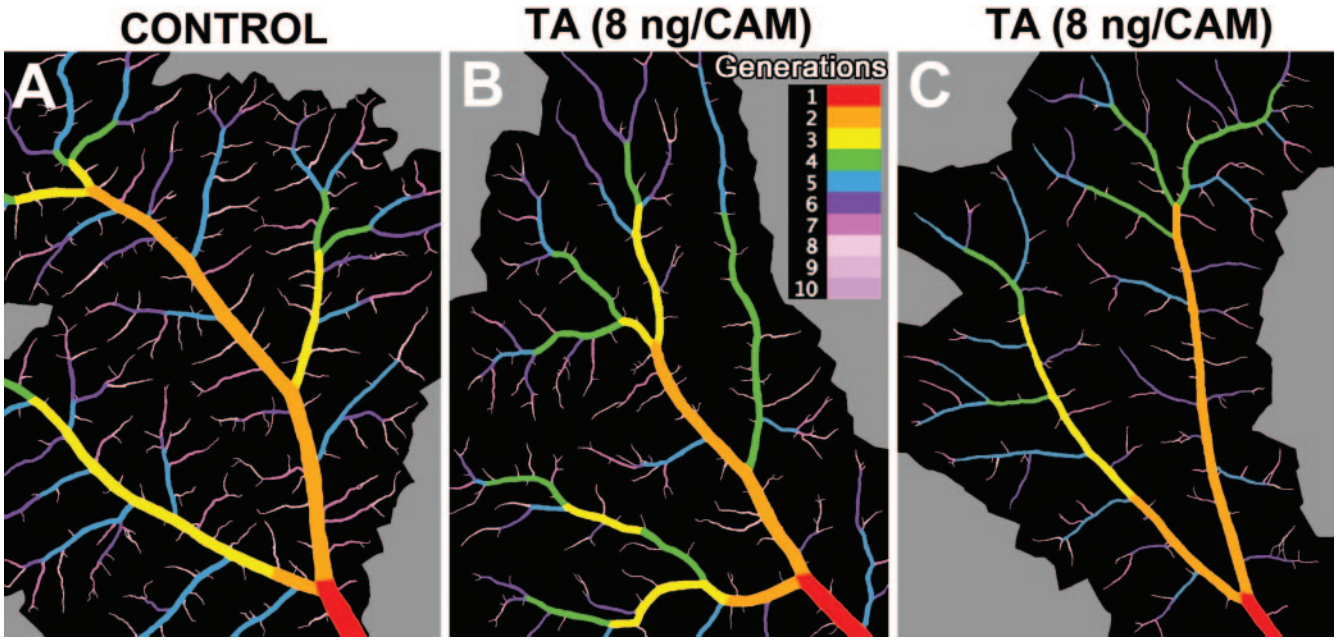

FIGURE 4. TA selectively decreases the number of smaller vessels and decreases vessel diameter throughout the vascular tree. (**A–C**) Each representative image displays the major arterial tree with its ROI (*black*) as determined by VESGEN, for which vessel diameter (D_v) and the density of key vascular parameters that included vessel number density (N_v), vessel branch point density (Br_v), vessel length density (L_v), and vessel area density (A_v) were measured. Parameters were specified for branching generations G_1–G_{10} (see colorized legend) and denoted D_{v1}, A_{v1}, L_{v1}, N_{v1}, etc. Relative to controls (**A**), VESGEN results for A_v, L_v, N_v, and Br_v in TA-treated specimens (**B–C**) showed that vessel density decreased only in the smallest branching generations G_7–G_{10} (Fig. 5). However, D_v decreased throughout vascular tree (Fig. 6). (**B**) VESGEN output image of the input binary image in Figure 1E.

stricted to smaller vessels and the overall thinning of vessel diameter. Vessel tortuosity as measured by T_v was unaffected, varying typically between 1.04 and 1.17 within a specimen. By N_v and L_v (Fig. 5), vessel density decreased significantly for the smallest vessels of G_7–G_{10} but not for large and medium-sized vessels of G_1–G_2, G_3–G_4, and G_5–G_6. N_{v7-10} decreased significantly from 474 ± 30 cm^{-2} in controls to 302 ± 33 cm^{-2} at 8 ng TA/CAM ($P = 0.0017$), whereas N_{v1-2}, N_{v3-4}, and N_{v5-6} remained relatively constant (Fig. 5; $P = 0.69$, 0.53, and 0.61, respectively). For example, N_{v1-2} was 5.04 ± 0.32 cm^{-2} in controls compared with 5.15 ± 0.05 cm^{-2} at 8 ng TA/CAM. Small but consistent decreases in vessel diameter (D_v) were induced by TA throughout the vascular tree (Fig. 6). D_{v7-10} decreased from 28.1 ± 1.0 μm in controls to 25.5 ± 0.4 μm at 8 ng TA/CAM ($P = 0.03$), D_{v5-6} from 61.1 ± 3.1 μm to 53.0 ± 3.1 μm ($P = 0.08$), D_{v3-4} from 118.1 ± 6.0 μm to 101.6 ± 5.8 μm ($P = 0.07$), and D_{v1-2} from 228.4 ± 12.1 μm to 199.0 ± 11.2 μm ($P = 0.09$).

A statistical study of the effects of vessel generational branching on our results confirmed the value and validity of site-specific VESGEN analysis. The binning (i.e., lumping or merging) of G_1–G_{10} output parameters demonstrated increasingly strong statistical confidence resulting from increasingly fine binning of the generational data. For example, measurements of D_v using a twofold binning of generations for controls and 8 ng TA/CAM into larger vessels of D_{v1-6} and smaller

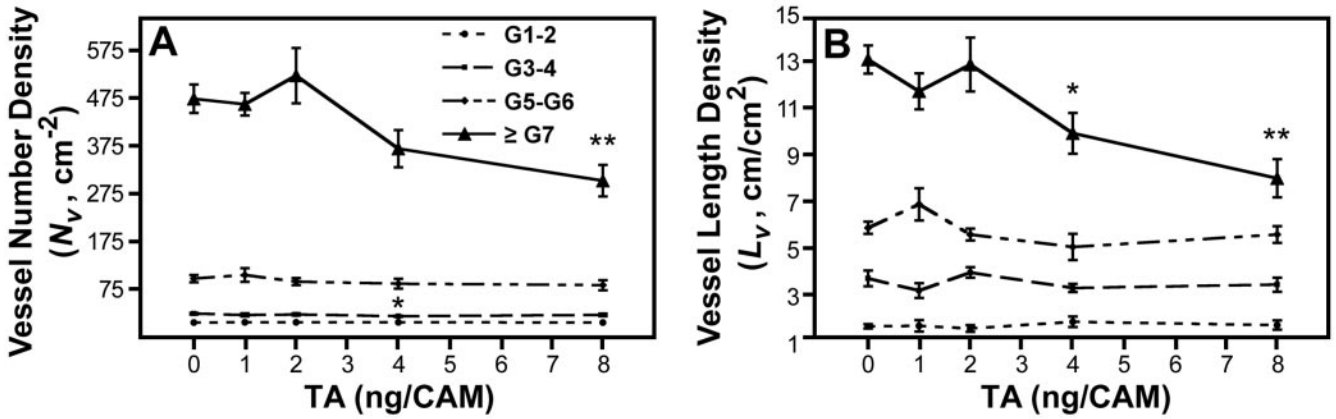

FIGURE 5. TA selectively inhibits the angiogenesis of small blood vessels. Relative to controls, vessel density estimated by vessel number density (N_v) and vessel length density (L_v) decreased only in the smallest branching generations G_7–G_{10} for higher concentrations of TA. For clarity, results for various classes of vessels lumped together as G_{1-2}, G_{3-4}, G_{5-6}, and $G_{\geq 7}$ (G_{7-10}). See Figures 1, 2, and 4 for qualitative confirmation of the quantitative results. Data are plotted as mean ± SE. $^*P \leq 0.05$. $^{**}P \leq 0.01$.

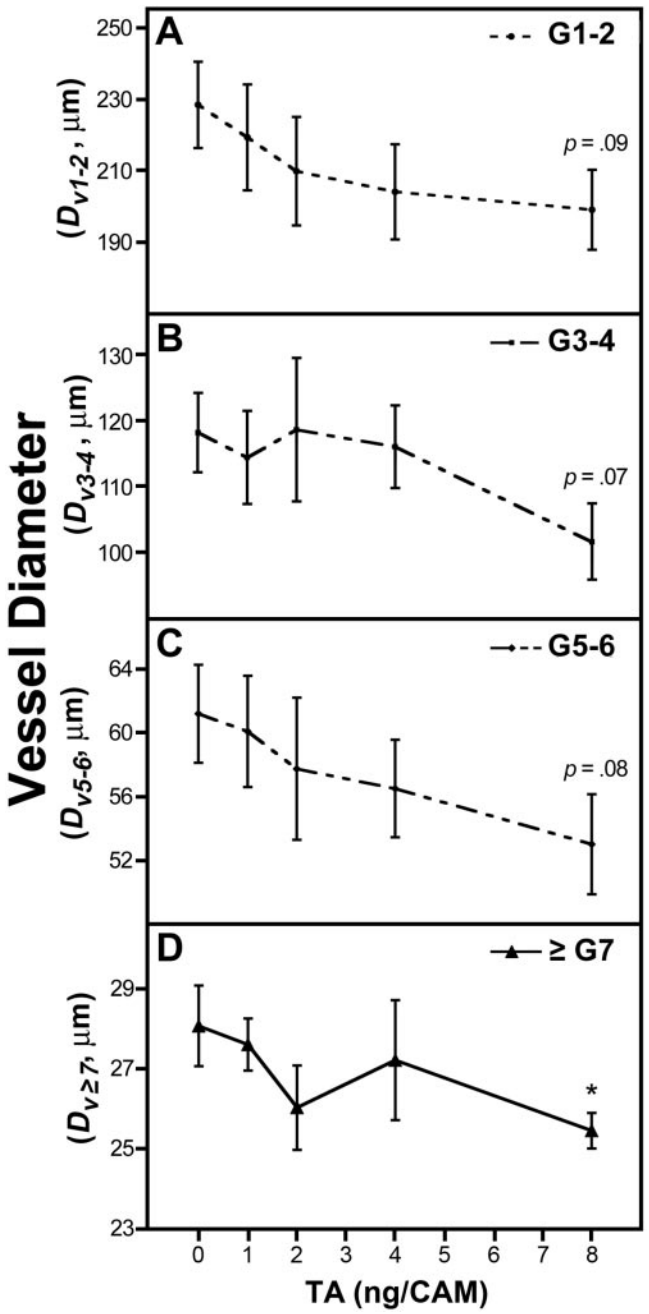

FIGURE 6. TA decreases vessel diameter throughout the vascular tree. Vessel diameter (D_v) decreased in all vessel branching generations (G_1–G_{10}) with increasing concentrations of TA compared with controls. As for Figure 5, results were lumped together as G_{1-2}, G_{3-4}, G_{5-6}, and $G_{\geq7}$ (G_{7-10}). For qualitative confirmation of quantitative results, see Figures 1 and 4. Data are plotted as mean ± SE. $^*P \leq 0.05$. $^{**}P \leq 0.01$.

vessels of D_{v7-10} (this group identical with results cited above) yielded a P value of relatively insignificant difference for the larger vessels ($P = 0.15$). Similarly, for a threefold binning of generations into D_{v1-3}, D_{v4-6}, and D_{v7-10}, P values for the two groups of larger vessels were also inconclusive ($P = 0.25$ and $P = 0.15$, respectively). As described, a finer fourfold binning of D_{v1-2}, D_{v3-4}, D_{v5-6}, and D_{v7-10} showed considerably higher levels of statistical significance for trends ($P \leq 0.10$) and confidence intervals ($P \leq 0.05$). Nonetheless, some binning of generational results, as performed for this study, improves and smooths the data because of increased statistical sampling[14,17] and provides greater clarity in the presentation of results.

DISCUSSION

Topical treatment with the corticosteroid TA resulted in multimodal changes to the vascular tree in the quail CAM, as quantified by VESGEN analysis. The angiogenesis of small blood vessels was selectively inhibited by TA, but vessel diameter decreased throughout the branching tree. Other critical aspects of vessel morphology remained normal after treatment by TA. For example, the density and number of larger vessels were unaffected, the vascular tree appeared to taper smoothly, and vessel tortuosity remained normal. It is not surprising that TA, as a potent angiogenesis inhibitor, selectively decreased the density of only small, new blood vessels within the vascular tree.[14] It is possible that TA decreased overall vessel diameter by inhibiting VEGF activity[6,7] because VEGF stimulates increases both in vessel diameter (particularly of larger vessels) and in vessel density.[17]

In this study, TA was applied topically to the quail CAM during mid-embryonic development, when angiogenesis is occurring at its maximum rate and angiogenic cytokines and regulators can be applied easily and uniformly in solution.[13–17] The transparent CAM membrane develops rapidly, is highly vascularized, and is essentially 2D. Complex spatial patterns of the branching vascular tree and associated capillary network are easily visualized by light and fluorescence/confocal microscopy and quantified by fractal-based VESGEN analysis. As a relatively convenient experimental model, the angiogenic CAM exhibits some useful morphologic and functional similarities to angiogenic diseases of the quasi-2D retinal vascular tree. For example, region-based fractal methods developed in the CAM were successfully extended to the quantification of progression in diabetic vascular disease using clinical images of the human retina.[21]

We are using the computer software VESGEN to quantify major vessel parameters of blood and lymphatic vascular remodeling. Output parameters of VESGEN include vessel diameter, tortuosity, fractal dimension, and densities of vessel number, branch point, length, and area. Most parameters can be obtained by the user for the overall vascular image, the major vascular tree, and individual or merged branching generations. Vascular trees are decomposed into branching generations so that cytokine- or therapeutic-regulated modifications can be quantified according to site-specific vessel location. For this study on TA, we chose to analyze generational branching within the major vascular tree. Focusing on branching relationships within a single tree can support precise conclusions about regulator-induced changes in vessel branching relationships. This is the first technical report of results generated by the fully mature, newly automated VESGEN software (version 1.0) that now analyzes 2D vascular trees, networks, and tree-network composites for a number of experimental and clinical tissue applications in angiogenesis and lymphangiogenesis, including the avian CAM and yolk sac, the human retina, rodent retina, and developing coronary vessels in the embryonic heart.

As demonstrated by VESGEN analysis, it now appears that perturbation of rapid, ongoing angiogenesis during the middle stages of CAM development by TA occurs primarily by the selective inhibition or stimulation of new, small blood vessels. As a generalized result for the CAM model, this conclusion appears important, though not particularly surprising, because the molecular and cellular characteristics of angiogenic vascular tissues differ from those of more mature, stable vascular tissues.[25,26] Angiogenic perturbants quantified to date in this

fractal-based CAM model include the inhibitors TA, transforming growth factor β-1 (TGF-β1)[14] and angiostatin,[13] and stimulators basic fibroblast growth factor (bFGF)[15] and vascular endothelial growth factor-165 ($VEGF_{165}$).[17] Additional regulator-specific effects on vascular morphology, such as overall vessel thinning by TA or thickening of larger blood vessels by $VEGF_{165}$, have also been quantified. As for TA, morphologic response of the vascular tree to $VEGF_{165}$ measured by VESGEN was multimodal. Increased vessel density and increased vessel diameter reached maximal frequencies at lower and higher VEGF concentrations, respectively. The study of TGF-β1 in particular considered tissue growth (rescaling) of the entire CAM vascular tree. Each molecular perturbant of angiogenesis has therefore elicited a unique "fingerprint" response that is spatiotemporally distinct and quantifiable, despite the apparent generality of inhibition and stimulation of angiogenesis in the CAM at the level of new, small vessels within the growing vascular tree.

Acknowledgments

The authors thank undergraduate summer interns Jennifer Kirsop (Lewis Educational and Collaborative Internship Program [LERCIP]), Elizabeth Locklear (American Indian Science and Engineering Society), and Leah Strazisar (LERCIP) for their research contributions.

References

1. Floman N, Zor U. Mechanism of steroid action in ocular inflammation: inhibition of prostaglandin production. *Invest Ophthalmol Vis Sci*. 1977;16:69–73.
2. Umland SP, Nahrebne DK, Razac S, et al. The inhibitory effects of topically active glucocorticoids on IL-4, IL-5, and interferon-gamma production by cultured primary $CD4^+$ T cells. *J Allergy Clin Immunol*. 1997;100:511–519.
3. Kang BS, Chung EY, Yun YP, et al. Inhibitory effects of anti-inflammatory drugs on interleukin-6 bioactivity. *Biol Pharm Bull*. 2001;24:701–703.
4. Sze PY, Iqbal Z. Glucocorticoid action on depolarization-dependent calcium influx in brain synaptosomes. *Neuroendocrinology*. 1994;59:457–465.
5. Sze PY, Iqbal Z. Glucocorticoid actions on synaptic plasma membranes: modulation of [125I]calmodulin binding. *J Steroid Biochem Mol Biol*. 1994;48:179–186.
6. Bandi N, Kompella UB. Budesonide reduces vascular endothelial growth factor secretion and expression in airway (Calu-1) and alveolar (A549) epithelial cells. *Eur J Pharmacol*. 2001;425:109–116.
7. Fischer S, Renz D, Schaper W, Karliczek GF. In vitro effects of dexamethasone on hypoxia-induced hyperpermeability and expression of vascular endothelial growth factor. *Eur J Pharmacol*. 2001;411:231–243.
8. Wilson CA, Berkowitz BA, Sato Y, Ando N, Handa JT, de Juan E Jr. Treatment with intravitreal steroid reduces blood-retinal barrier breakdown due to retinal photocoagulation. *Arch Ophthalmol*. 1992;110:1155–1159.
9. Kaiser PK. Steroids for branch retinal vein occlusion. *Am J Ophthalmol*. 2005;139:1095–1096.
10. Margolis R, Singh RP, Kaiser PK. Branch retinal vein occlusion: clinical findings, natural history, and management. *Compr Ophthalmol Update*. 2006;7:265–276.
11. Brasil OF, Smith SD, Galor A, Lowder CY, Sears JE, Kaiser PK. Predictive factors for short-term visual outcome after intravitreal triamcinolone acetonide injection for diabetic macular oedema: an optical coherence tomography study. *Br J Ophthalmol*. 2007;91:761–765.
12. Taban M, Singh RP, Chung JY, Lowder CY, Perez VL, Kaiser PK. Sterile endophthalmitis after intravitreal triamcinolone: a possible association with uveitis. *Am J Ophthalmol*. 2007;144:50–54.
13. Parsons-Wingerter P, Lwai B, Yang MC, et al. A novel assay of angiogenesis in the quail chorioallantoic membrane: stimulation by bFGF and inhibition by angiostatin according to fractal dimension and grid intersection. *Microvasc Res*. 1998;55:201–214.
14. Parsons-Wingerter P, Elliott KE, Farr AG, Radhakrishnan K, Clark JI, Sage EH. Generational analysis reveals that TGF-beta1 inhibits the rate of angiogenesis in vivo by selective decrease in the number of new vessels. *Microvasc Res*. 2000a;59:221–232.
15. Parsons-Wingerter P, Elliott KE, Clark JI, Farr AG. Fibroblast growth factor-2 selectively stimulates angiogenesis of small vessels in arterial tree. *Arterioscler Thromb Vasc Biol*. 2000b;20:1250–1256.
16. Parsons-Wingerter P, McKay TL, Leontiev D, Vickerman MB, Condrich TK, Dicorleto PE. Lymphangiogenesis by blind-ended vessel sprouting is concurrent with hemangiogenesis by vascular splitting. *Anat Rec A Discov Mol Cell Evol Biol*. 2006a;288:233–247.
17. Parsons-Wingerter P, Chandrasekharan UM, McKay TL, et al. A VEGF165-induced phenotypic switch from increased vessel density to increased vessel diameter and increased endothelial NOS activity. *Microvasc Res*. 2006b;72:91–100.
18. Mandelbrot BB. *The Fractal Geometry of Nature*. San Francisco: W. H. Freeman; 1983.
19. Bassingthwaighte JB, Liebovitch LS, West BJ. *Fractal Physiology*. New York: Oxford University Press; 1994.
20. West GB, Brown JH, Enquist BJ. A general model for the origin of allometric scaling laws in biology. *Science*. 1997;276:122–126.
21. Avakian A, Kalina RE, Sage EH, et al. Fractal analysis of region-based vascular change in the normal and non-proliferative diabetic retina. *Curr Eye Res*. 2002;24:274–280.
22. Gan RZ, Tian Y, Yen RT, Kassab GS. Morphometry of the dog pulmonary venous tree. *J Appl Physiol*. 1993;75:432–440.
23. Kassab GS, Rider CA, Tang NJ, Fung YC. Morphometry of pig coronary arterial trees. *Am J Physiol*. 1993;265:H350–H365.
24. Kassab GS, Lin DH, Fung YC. Morphometry of pig coronary venous system. *Am J Physiol*. 1994;267:H2100–H2113.
25. Benjamin LE, Hemo I, Keshet E. A plasticity window for blood vessel remodelling is defined by pericyte coverage of the preformed endothelial network and is regulated by PDGF-B and VEGF. *Development*. 1998;125:1591–1598.
26. Gerhardt H, Golding M, Fruttiger M, et al. VEGF guides angiogenic sprouting utilizing endothelial tip cell filopodia. *J Cell Biol*. 2003;161:1163–1177.